Clays and Clay Minerals, Vol. 49, No. 1, 60–72, 2001.

PROPERTIES AND ACID DISSOLUTION OF METAL-SUBSTITUTED HEMATITES

M.A. WELLS,[1] R.J. GILKES,[2] AND R.W. FITZPATRICK[3]

[1] CSIRO Exploration and Mining, Wembley, Perth, Western Australia, 6913, Australia
[2] Department of Soil Science and Plant Nutrition, University of Western Australia, Perth, Western Australia, 6907, Australia
[3] CSIRO, Land and Water, Glen Osmond, Adelaide, South Australia, 5064, Australia

Abstract—The dissolution in 1 M HCl of Al-, Mn-, and Ni-substituted hematites and the influence of metal substitution on dissolution rate and kinetics of dissolution were investigated. The inhomogeneous dissolution of most of the hematites investigated was well described by the Avrami-Erofe'ev rate equation, $kt = \sqrt{[-\ln(1 - \alpha)]}$, where k is the dissolution rate in time, t, and α is the Fe dissolved. Dissolution of Al-substituted hematite occurred mostly by edge attack and hole formation normal to (001), with the rate of dissolution, k, directly related to surface area (SA). Dissolution of rhombohedral Mn- and Ni-bearing hematites occurred at domain boundaries, crystal edges, and corners with k unrelated to SA. The morphology of Mn- and Ni-substituted hematites changed during dissolution with clover-leaf-like forms developing as dissolution proceeded, whereas the original plate-like morphology of Al-bearing hematite was generally retained. Acid attack of platy and rhomboidal hematite is influenced by the direct (*e.g.*, metal-oxygen bond energy, hematite crystallinity) and indirect (*e.g.*, crystal size and shape) affects associated with incorporation of foreign ions within hematite.

Key Words—Acid Dissolution, Activation Energy, Frequency Factor, Hematite, Iron Oxide, Metal Substitution.

INTRODUCTION

Goethite (α-FeOOH) and hematite (α-Fe_2O_3) are two of the most commonly occurring Fe-oxides in soils and sediments. These Fe-oxides act as sinks for trace and heavy metals during soil formation (Kuhnel, 1987) so that during their dissolution in the soil Fe and associated metal ions may be introduced into the soil solution (Schwertmann and Taylor, 1989). This process is of importance to fields as diverse as environmental chemistry (Sulzberger *et al.*, 1989; Schwertmann, 1991) and geochemical exploration (Sidhu *et al.*, 1981). Acid and ligand dissolution of Fe-oxides such as magnetite and hematite has also been studied in relation to the descaling of reactor cooling pipes (Segal and Sellers, 1981; Baumgartner *et al.*, 1983).

Numerous studies have investigated the dissolution kinetics of natural and synthetic Fe-oxides to characterize the mechanism of Fe-oxide dissolution in relation to chemical weathering and the rate of release of trace metals into solution (Pryor and Evans, 1950; Cornell *et al.*, 1975; Sidhu *et al.*, 1981; Cornell and Schindler, 1987). The mechanisms of dissolution of pure and Al-substituted, synthetic and natural goethite in 1 M HCl solutions are well understood (Surana and Warren, 1969; Cornell *et al.*, 1974, 1975, 1976; Schwertmann, 1984; Cornell and Schindler, 1987). The acid dissolution of goethite containing foreign ions other than Al that replace Fe has also received attention (Lim-Nunez and Gilkes, 1987).

Investigations of the acid (*i.e.*, H^+) dissolution of hematite have mainly involved unsubstituted synthetic (Cornell and Giovanoli, 1993) and natural (Warren *et al.*, 1969; Segal and Sellers, 1980) samples. It is only recently that elements other than Al, such as Mn (Vandenberghe *et al.*, 1986) and Ni (Cornell *et al.*, 1992), were also shown to replace Fe within hematite and their influence on the mineralogical properties of hematite investigated. The dissolution of metal-substituted hematites in acid (H^+) media has, however, received little attention. The present study investigates the dissolution in HCl of a range of Al-, Mn-, and Ni-substituted hematites.

MATERIALS AND METHODS

Pure and metal-substituted hematites were prepared from (Al, Mn, Ni)-ferrihydrites based on the methods of Fischer and Schwertmann (1975) and Schwertmann and Murad (1983). Metal-ferrihydrites were prepared from mixed Fe^{3+}-Al^{3+}, Fe^{3+}-Mn^{2+}, and Fe^{3+}-Ni^{2+} nitrate solutions via addition of 4 M NH_4OH to ~30% excess of the stoichiometric quantity required to coprecipitate the metal-ferrihydrite gel. Nominal amounts of mole% Al-, Mn-, and Ni-substitution are given in Table 1. The gels were collected by centrifugation, washed three times with 200 mL deionized water and transferred to 1.0-L stoppered-glass reagent bottles and resuspended in 900 mL deionized (DI) water adjusted to pH 7.5–8.0. The suspensions were aged at 90°C for 14 d during which time the precipitates were mixed each day and the pH readjusted to 7.5–8.0 using either 0.2 M KOH or 0.5 M HCl. After aging, the solid material was washed with DI water and dried from acetone at 40°C.

Table 1. Mineral properties of metal-substituted hematites.

Initial mole %	Actual mole[1] %	Munsell color (dry)	a (nm)[2]	c (nm)[2]	Wt. loss (%)[3]	SA ($m^2\ g^{-1}$)	MCL_a (nm)	MCL_c (nm)[4]
[5]0	0	na	0.5030 (5)	1.3747 (8)	na	na	24.6	31.2 (1.0)
	(Al)							
5	4.6	10R 4/8	0.5023 (5)	1.3732 (7)	0.9	18	26.5	35.4 (6.5)
10	8.3	10R 4/8	0.5016 (5)	1.3716 (8)	2.1	24	23.4	19.3 (3.5)
15	13.4	10R 4/8	0.5011 (5)	1.3720 (8)	4.6	36	18.7	7.3 (1.9)
20	15.0	10R 4/8	0.5008 (6)	1.3692 (15)	5.8	45	15.8	4.8 (0.9)
	(Mn)							
4	3.3	2.5YR 3/4	0.5033 (5)	1.3751 (7)	1.3	17	na	35.3 (20)
8	6.3	1.25YR 3/4	0.5036 (6)	1.3746 (10)	1.7	18	22.1	21.3 (9.4)
	(Ni)							
3	1.1	8.75R 4/8	0.5031 (5)	1.3757 (8)	1.3	16	37.6	26.7 (8.4)
5	1.8	8.75R 4/8	0.5035 (5)	1.3761 (7)	1.6	15	38.7	36.8 (20)
7	2.4	8.75R 4/8	0.5034 (5)	1.3763 (8)	1.7	14	59.6	41.2 (17)
15	6.0	8.75R 4/8	0.5040 (5)	1.3783 (8)	2.2	14	42.0	45.2 (17)

[1] mole % metal = [Me/(Me + Fe)] × 100.
[2] Standard deviations for the last significant figure for unit-cell values are given in parentheses.
[3] Weight loss determined for the interval 105–700°C.
[4] Values in parentheses are the standard deviation of MCL_c values.
[5] Control sample contains geothite also. All other samples are hematite only.
na: Data was not available.

Amorphous material was removed by two, 60-min treatments with acid (pH 3.0) ammonium-oxalate extractions in the dark (McKeague and Day, 1966) using a sample to solution ratio of 1:200. The samples were washed thoroughly with DI water to remove salts and again dried from acetone before further analysis.

X-ray diffraction (XRD) analysis was conducted using a Philips PW 1050 vertical goniometer with 1° receiving and divergence slits and graphite diffracted-beam monochromator with CuKα radiation. XRD patterns were obtained by step-scanning powder samples at 0.3 °2θ/min in 0.01 °2θ steps at a counting time of 2 s/step, with 10% NaCl added as an internal standard, for accurate determinations of spacings and line broadening.

Unit-cell parameters were calculated from positions of the (012), (104), (113), (024), (116), (018), (214), and (300) reflections of hematite, and the *least-squares* procedure of Novak and Colville (1989). The standard deviations for a and c dimensions determined in this way were larger than those obtained by others, but there were no anomalous Q values for the refined patterns. Thus, the standard deviation must reflect the error associated with the measurement of d values of broad reflections. The parameter Q ($= 1/d^2_{obs}$) is used as an indication of any systematic errors (*i.e.*, goniometer misalignment) introduced in the unit-cell refinement (Novak and Colville, 1989).

The size of coherently diffracting domains (mean coherence length, MCL) along the a and c axes was calculated from the Scherrer equation (Klug and Alexander, 1974) using a K value of 0.9 for those reflections corrected for line broadening. MCL_a was obtained from values of MCL_{300}. Values of MCL_c were obtained by multiplication of MCD_{hkl} by cos ψ, where ψ is the angle between the vector perpendicular to the *hkl* plane and the [001] direction.

Surface areas of oxalate-treated hematites were obtained using the (BET) N_2 single-point adsorption method. Thermogravimetric analysis (TGA) was performed using a Perkin Elmer TGS-2 thermo-balance. Ten-milligram powdered samples were heated in a Pt crucible from 60 to 700°C at 10°C/min under dry air flowing at 15–20 mL/min. Munsell colors of oxalate-treated hematites were recorded following the recommendations of Melville and Atkinson (1985).

Sequential acid dissolution was conducted using 10-mg samples in 22 mL of 1.0 M HCl in 25-mL polythene vials. Acid aliquots were added using a calibrated dispenser. The suspensions were placed in a controlled-environment incubator shaker and shaken at 400 cpm (cycles per minute). Previous work indicated that for shaking speeds >200 cpm, dissolution is not diffusion controlled and depends solely on the surface-reaction rate (Cornell *et al.*, 1974). Initially, 2-mL aliquots were withdrawn from the suspensions at selected times using a calibrated pipette and filtered using 0.22-μm cellulose nitrate membranes. As dissolution continued for longer shaking times, 0.5-mL aliquots were withdrawn, using a calibrated pipette for analysis to maintain an adequate volume of acid. Previous dissolution studies used a solution to solid ratio in the range 250–2000:1 (Cornell *et al.*, 1974, 1992; Sidhu *et al.*, 1981; Lim-Nunez and Gilkes, 1987) to ensure that dissolution was independent of the solution to sample ratio (Cornell *et al.*, 1974; Sidhu *et al.*,

https://doi.org/10.1346/CCMN.2001.0490105 Published online by Cambridge University Press

Table 2. Stereochemical properties of metal ions in octahedral coordination.

Ion	Metal-oxygen bond energy [1](kJ/mole)	Ionic radius [2](nm)	Octahedral CFSE [3](kJ/mole)	Site-preference energy [3](kJ/mole)
Al^{3+}	512.1	0.0535	—	—
Fe^{3+}	390.4	0.0645	0	0
Mn^{3+}	402.9	0.0645	150.6	105.9
Ni^{2+}	382.0	0.069	123.8	95.4

[1] *Handbook of Chemistry and Physics* (1988).
[2] Shannon (1976).
[3] Burns (1970).

1981). The solution to solid ratio in the present study was 2200:1. Determinations of dissolved Fe, Al, Mn, and Ni were performed using a Perkin Elmer 403 atomic adsorption spectrophotometer (AAS). Sample duplicates and blanks were included as a check on reliability of the data.

Activation-energy (E) and frequency-factor (A) kinetic data were obtained from results for dissolution at 40, 50, and 60°C. Much of the previous work regarding acid dissolution of Fe-oxides, such as goethite, hematite, and magnetite, was conducted using ~1 M HCl solutions at temperatures between 40–90°C (Warren *et al.,* 1969; Cornell *et al.,* 1974, 1975; 1976; Sidhu *et al.,* 1981; Schwertmann, 1984). These conditions were used because the reaction products are simple and well understood, and so that dissolution experiments can be completed within a reasonable time. Similar conditions of temperature, acid type, and concentration (*i.e.,* 1.0 M HCl) are used here to enable comparisons with published data.

Transmission electron microscopy (TEM) of original and partially dissolved (~35 mole % Fe) hematite was performed using a Philips 430 analytical transmission electron microscope (ATEM) operating at 300 kV. For TEM examination, samples were prepared by air-drying suspensions onto carbon-coated copper grids.

RESULTS AND DISCUSSION

Sample characterization

XRD analysis indicated that the unsubstituted control sample consisted of a mixture of goethite and hematite. The formation of goethite during hematite synthesis has been previously reported (Johnston and Lewis, 1983; Schwertmann and Murad, 1983), and this sample was not used for further analysis except for unit-cell parameter and crystallite-size determinations (Table 1). XRD indicated that all metal-substituted samples consisted of only monomineralic hematite, to within the detection limit (~5%) of XRD analysis.

The unit-cell *a* value for unsubstituted hematite of 0.5030 nm is slightly smaller than some reported values (Schwertmann and Taylor, 1989). Unit-cell dimensions of Al-rich hematites decreased with increasing Al substitution [$a = 0.5029 - 1.42 \times 10^{-3}$ (mole % Al), $r^2 = 0.990$***; $c = 1.3746 - 2.97 \times 10^{-3}$ (mole % Al), $r^2 = 0.81$**, Table 1, where ** represents a 95% confidence level, and *** indicates a 99% confidence level], which is consistent with incorporation of the smaller Al^{3+} ion (Table 2). Contraction of unit-cell parameters is less than that predicted by the Vegard relationship, which is consistent with reported data for synthetic Al-substituted hematites (Schwertmann *et al.,* 1979; DeGrave *et al.,* 1988; Wells *et al.,* 1989). This difference is related partly to the presence of structural defects and to incorporation of structural H_2O (Table 1), with OH^- replacing O^{2-} ions (Stanjek and Schwertmann, 1992). Unit-cell dimensions of Ni-bearing hematite were positively related to Ni-substitution [$a = 0.5030 + 1.71 \times 10^{-3}$ (mole % Ni), $r^2 = 0.93$***; $c = 1.3749 - 5.77 \times 10^{-3}$ (mole % Ni), $r^2 = 0.986$***, Table 1], which is consistent with incorporation of the larger Ni^{2+} ion (Table 2). A similar increase in the *a* dimension was reported for synthetic Ni-substituted hematites containing ≤7 mole % Ni (Cornell *et al.,* 1992). Incorporation of Ni^{2+} may involve a coupled substitution with OH^- replacing O^{2-} ions, *i.e.,* $Fe_2O_3 \rightarrow Fe^{3+}Ni^{2+}O_2OH$. This associates half a mole of water with each mole of Ni. Thus, hematite containing 6.0 mole % Ni, which is equivalent to 0.07 mole Ni/100 g, is associated with 2.2 wt. % H_2O or 0.12 moles H_2O/100 g.

Manganese-substituted hematites are dark reddish-brown to dark red in color, and are much darker than either Al- or Ni-substituted hematites (Table 1). Unit-cell parameters of Mn-rich hematites were not significantly different from those for the unsubstituted control hematite (Table 1). This may be related to incorporation of Mn^{3+} within hematite; Mn^{3+} and Fe^{3+} have very similar ionic radii (Table 2). For hematite synthesis, manganese was added as the manganous, Mn^{2+}, ion. In the case of Mn-substituted goethite produced from ferrihydrite, incorporation of Mn^{2+} occurs via oxidation of surface adsorbed Mn^{2+}-species (Giovanoli and Cornell, 1992). Oxidation occurs at the surface of goethite where highly charged Fe^{3+} ions catalyze the oxidation of Mn^{2+} to Mn^{3+} before incorporation (Davies and Morgan, 1989). A similar mechanism may have occurred for Mn to replace Fe in hematite.

Goethite cannot be distinguished from hematite in the control samples because no discerning morphologies were identified in the TEM micrographs. Hematite with low Al contents consisted of pseudo-hexagonal particles of ~140 nm in diameter (Figure 1). Incorporation of 15 mole % Al resulted in preferential crystal growth along the [100] direction (*i.e.,* crystal width) producing irregularly shaped, platy particles of ≤900 nm in size, at the expense of crystal thickness (Figure 1). Hematite containing low levels of Mn and Ni consisted of small (~140–150 nm) subhedral, aggregated particles. Larger amounts of Mn and Ni pro-

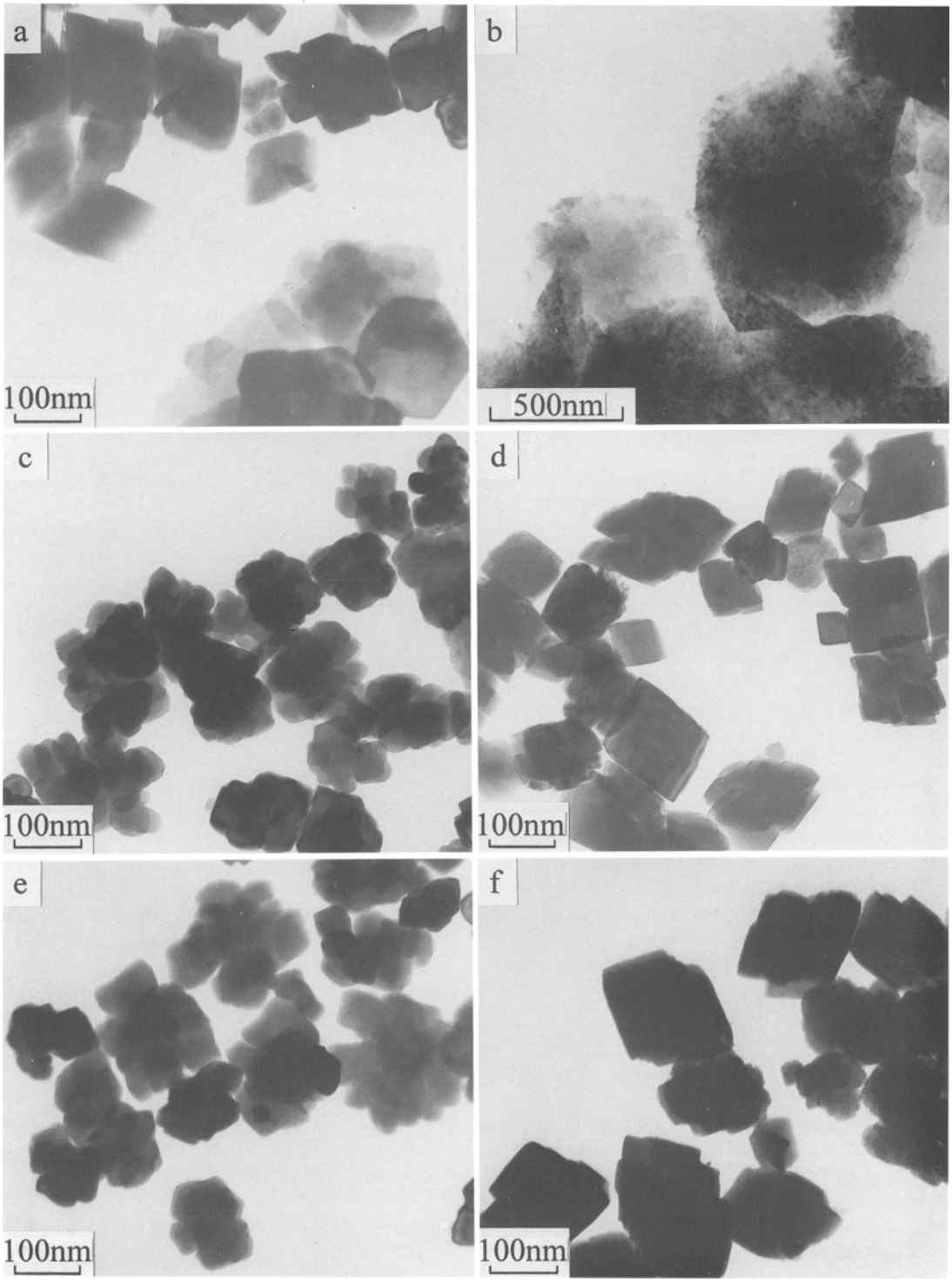

Figure 1. Transmission electron micrographs of low (a) Al-, (c) Mn-, and (e) Ni-substituted hematite, and high (b) Al-, (d) Mn-, and (f) Ni-substituted hematite. Owing to the plate-like nature of Al-substituted hematite only changes along the [100] direction (*i.e.*, crystal width) can be observed by TEM.

https://doi.org/10.1346/CCMN.2001.0490105 Published online by Cambridge University Press

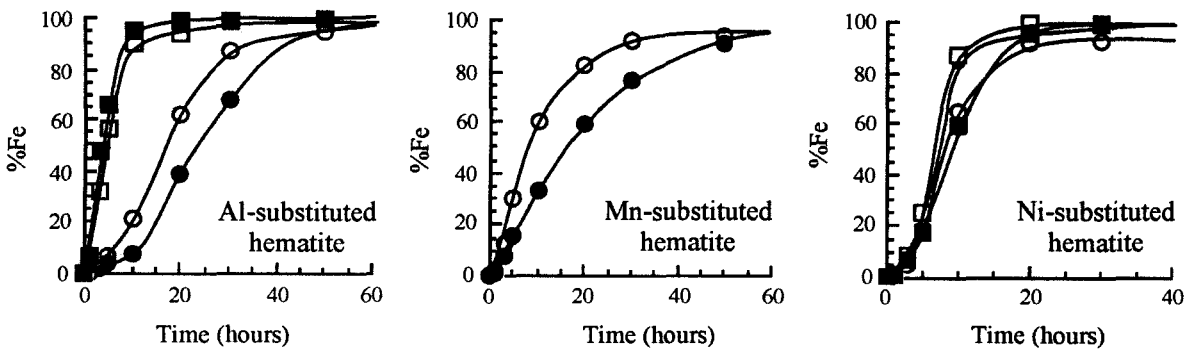

Figure 2. Dissolution-time curves for % of total Fe dissolved for Al-, Mn-, and Ni-substituted hematites dissolved in 1 M HCl at 60°C. For Al-bearing hematites (○) 4.6 mole %, (●) 8.3 mole %, (□) 13.4 mole %, (■) 15.0 mole %; Mn-bearing hematites (○) 3.3 mole %, (●) 6.3 mole %; Ni-bearing hematites (○) 1.1 mole %, (●) 1.8 mole %, (□) 2.4 mole %, (■) 6.0 mole %.

duced fewer irregularly shaped crystals with more equant, rhomboidal forms of ~130 nm in size (Figure 1), which were similar in size to rhomboidal hematites produced at pH 8–9 from ferrihydrite (Cornell and Giovanoli, 1989, 1993).

Values of MCL of domains along the [100] direction of Al-, Mn-, and Ni-substituted hematites (Table 1) determined from XRD line-broadening measurements were less than particle sizes as determined by TEM. This suggests that hematite crystals contain many domains with a substructure consisting of (several) smaller (*e.g.,* 30–40 nm, for hematite containing Ni) crystallites or domains. The presence of such a substructure could not be discerned from micrographs of Mn- and Ni-substituted hematites or for hematite containing 4.6 mole % Al (Figure 1). The mottled appearance of hematite containing 15 mole % Al (Figure 1b) may indicate the presence of a substructure, although this may also be a relic feature inherited from the primary structure of the precursor ferrihydrite (Cornell *et al.,* 1987).

Kinetics of acid dissolution

Dissolution curves obtained during the first 5–10 h of dissolution for hematites with Al contents of 4.6 and 8.3 mole %, and Ni-substituted hematites showed sigmoidal behavior. Thereafter, dissolution for all metal-substituted hematites followed a decelerating trend to completion of the reaction (Figure 2). The data presented in Figure 2 are for dissolution at 60°C. Dissolution (*i.e.,* % Fe dissolved *versus* time) curves for metal-substituted hematites at 40 and 50°C also showed similar decelerating trends (not shown).

Sigmoidal dissolution has been described for natural (Warren *et al.,* 1969; Warren and Roach, 1971) and synthetic hematites (Azuma and Kametani, 1964; Cornell and Giovanoli, 1993). The dissolution rate of hematite is considered independent of particle morphology with sigmoidal dissolution attributed to the initial slow reaction of dissolution sites (Cornell and Giovanoli, 1993).

The Cube Root Law (Cornell *et al.,* 1975) did not apply to the dissolution of metal-substituted hematites as samples showed sigmoidal or decelerating dissolution. This result implies that dissolution is either incongruent or that two (or more) discrete phases may be present (Lim-Nunez and Gilkes, 1987). XRD and thermal analysis, however, did not detect any additional phases in these samples indicating that hematite dissolution was inhomogeneous.

Such dissolution behavior was successfully described by the Avrami-Erofe'ev equation, $kt = \sqrt{[-\ln(1-\alpha)]}$, where α is the fraction of Fe dissolved at time t (min) and k is the dissolution rate (min^{-1}) (Cornell and Giovanoli, 1993). The dissolution rate may be conveniently obtained from the slope of the plot of $\sqrt{[-\ln(1-\alpha)]}$ *versus* time. This equation is based on the assumption that dissolution is surface controlled with random initiation of dissolution sites (Cornell and Giovanoli, 1993). The Avrami-Erofe'ev equation successfully described 87–100 mole % Fe (r^2 = 0.97) dissolved for Al-rich hematite and also applied to the initial 70–90 mole % Fe dissolved for Ni-substituted hematite and hematite containing 6.3 mole % Mn (Figure 3). However, the Avrami-Erofe'ev equation did not apply to the dissolution of hematite containing 3.3 mole % Mn (Figure 3).

The dissolution rate of Al-substituted hematites showed a general increase with increasing amounts of Al (Table 3). This rate occurred despite the larger Al-O bond energy relative to the Fe-O bond (Table 2) and may reflect the increase in SA of hematite (Table 1), which would be susceptible to proton attack. By contrast, studies on the reductive dissolution of synthetic hematites, with Al contents similar to the present study, reported a decrease in the dissolution rate with increasing Al substitution (Torrent *et al.,* 1987). For natural samples, reductive dissolution preferentially

https://doi.org/10.1346/CCMN.2001.0490105 Published online by Cambridge University Press

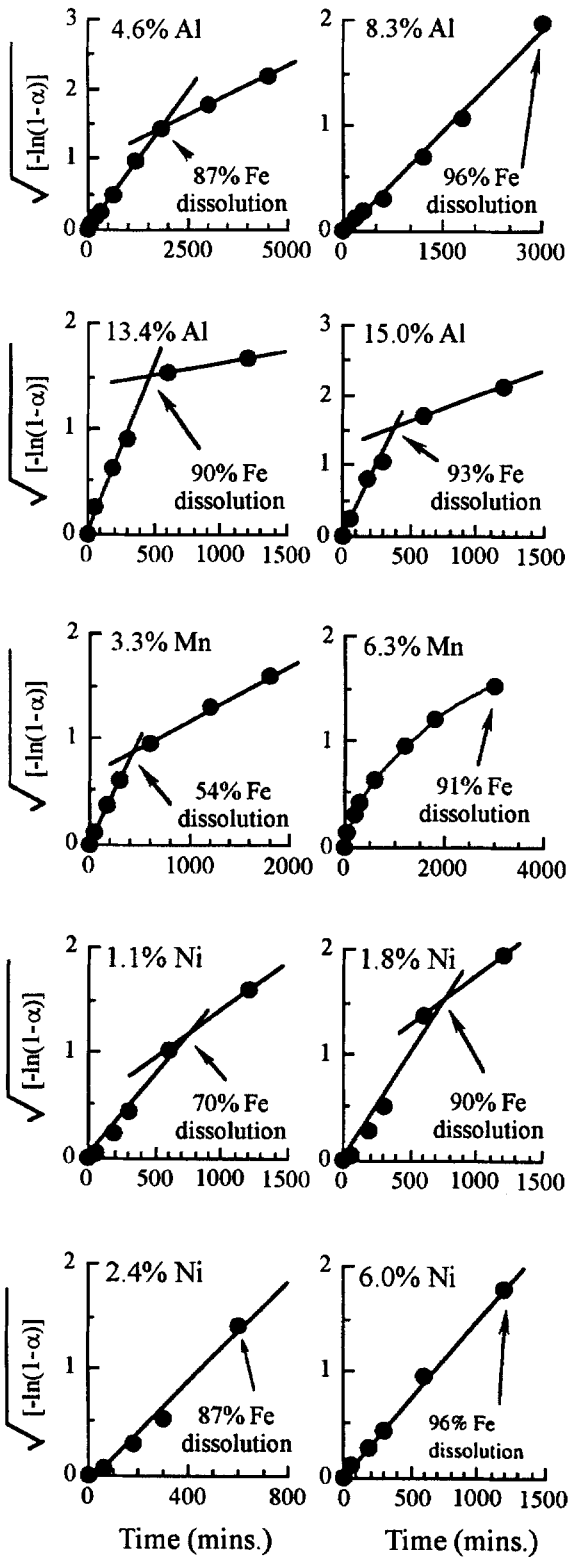

removes hematite with low amounts of Al relative to goethite with high Al contents (Macedo and Bryant, 1989; Jeanroy *et al.,* 1991). This result, in light of the present work, suggests that for the reductive dissolution of Al-rich hematite the detachment of Al is the rate-limiting step; the rate of reductive dissolution is not influenced by effects of the substitution of Al on the size or shape of hematite (*i.e.,* the greater the Al content the slower the dissolution). Dissolution rates for Ni-bearing hematites were unrelated to increasing amounts of Ni (Table 3).

Sigmoidal dissolution-time curves may also be described by the equation of Kabai (1973), $C = 1 - e^{-Kt\alpha}$, where C is the fraction of Fe dissolved at time t, and K and α are constants. This equation is an extension of the pseudomonomolecular-reaction equation where α becomes unity (Schwertmann *et al.,* 1985). The equation of Kabai (1973) in its linear form, $\ln\ln[1/(1 - C)] = \ln K + \alpha \ln t$, better described the dissolution of most Mn- and Ni-substituted hematite than the Avrami-Erofe'ev equation, but it did not extend to Al-substituted hematites or hematite containing 3.3 mole % Mn (Figure 4).

The dissolution rate, k, for Al-substituted hematite derived from the Avrami-Erofe'ev equation was positively related to surface area (Table 3). In contrast, dissolution rates for Ni-rich hematite, derived from the Kabai and Avrami-Erofe'ev equations, were not related to surface area (Table 3). This result differs from that for unsubstituted hematites where dissolution was independent of morphology with k being directly proportional to SA (Cornell and Giovanoli, 1993).

Activation energy and frequency factor

Activation-energy (E) and frequency-factor (A) values for substituted hematites were derived from the Arrhenius equation, in linearized form, $\ln K2 = \ln A - E/RT$, with R the universal gas constant, K2 a rate constant, and T the absolute temperature (Table 3). For the acid dissolution of Fe-oxides, E relates to the ionic properties of Fe and the substituent element, including such properties as electronegativity, bond strength, and ionic potential. The frequency factor incorporates the effects of acid concentration, density of dissolution sites over the crystal surface and, for dissolution in HCl, a Cl^- adsorption factor (Cornell *et al.,* 1974). The rate constant K2, with units $gFe/m^2/h$, was derived from the initial portion (*i.e.,* <5 mole % Fe dissolved)

←

Figure 3. Linearized plots of % of total Fe dissolved *versus* time for Al-, Mn-, and Ni-substituted hematites fitted to the Avrami-Erofe'ev equation. An arrow indicates the percentage dissolution at which dissolution kinetics may cease to be fully described by the equation. All fitted lines to this point have r^2 values of ≥0.97. An interpolated line is fitted to the dissolution data for hematite containing 6.3 mole % Mn.

https://doi.org/10.1346/CCMN.2001.0490105 Published online by Cambridge University Press

Table 3. Dissolution parameters, k and k2, for dissolution-times curves at 60°C for Al-, Mn-, and Ni-substituted hematites fitted to the Avrami-Erove'ev rate equation, and activation-energy (E) and frequency-factor (A) values.

Sample	k (min^{-1}) × 10^3	[1]k2 (min^{-1} m^2) × 10^3	[2]Regression coefficient	[3]Regression coefficient	E (kJ/mole)	A ($gFe/m^2/h$)
Al; 4.6%	0.796	0.044	0.92**[4]	0.86*[5]	75.5	3.96×10^8
8.3%	0.645	0.026			85.1	5.98×10^9
13.4%	2.99	0.082			76.1	1.03×10^9
15.0%	3.53	0.079			66.1	2.34×10^7
Mn; 3.3%	2.03	0.118	—	—	82.2	1.52×10^{10}
6.3%	0.498	0.028			84.1	2.04×10^{10}
Ni; 1.1%	1.75	0.106	0.02	0.19	71.0	1.18×10^8
1.8%	2.34	0.156			73.3	4.31×10^8
2.4%	2.40	0.172			81.6	1.17×10^{10}
6.0%	1.49	0.108			85.6	3.54×10^{10}

[1] Dissolution rate independent of surface area (*i.e.*, k2 = k/SA).
[2] Coefficient for the regression of k *vs.* SA.
[3] Coefficient for the regression of K, derived from dissolution-time curves of metal-hematites fitted to the equation of Kabai (1973), *versus* SA.
[4] **95% confidence limit.
[5] *90% confidence limit.

of the hematite dissolution-time curves (Figure 2), where the dissolution rate should not be greatly affected by changes in crystal morphology (*i.e.*, SA). The rate of hematite dissolution increased with increasing temperature (*i.e.*, from 40 to 60°C); the following discussion is only for dissolution at 60°C. Values of E and A were obtained graphically from the slope and intercept, respectively, of plots of lnK2 *vs.* 1/T, with r^2 values ≥0.91 (data not shown).

Activation-energy values for hematite of the present study are similar to reported values of 94.6–97.9 kJ/mole for the dissolution of synthetic and natural hematites (Azuma and Kametani, 1964; Warren and Roach, 1971; Sidhu *et al.*, 1981), although values as low as 41.8 kJ/mole were reported (Krestov *et al.*, 1973).

Changes in the activation energy of hematites relating to incorporation of Al were non-systematic and therefore, did not simply reflect the larger Al-O bond energy relative to the Fe-O bond or other stereochemical parameters (Table 2). The trend in E values with Al content may reflect a structural order/disorder effect. Maximum values of E occurred for Al contents of ~8 mole % (Table 3). The dissolution rates, k and k2, were also at a minimum for this amount of Al substitution (Table 3). Incorporation of 5–8 mole % Al increased grain and crystallite size along the [100] and [001] directions (Table 1) and therefore, presumably, increased hematite crystallinity (*i.e.*, structural order) associated with fewer structural defects. The result is an increase in activation energy and a reduction in the rate of hematite dissolution. A similar increase in hematite crystallinity was reported for other synthetic hematites containing ~5 mole % Al and is considered a consequence of the reduction in lattice-strain energy relating to incorporation of the smaller Al^{3+} ion within hematite (Schwertmann *et al.*, 1979). A similar effect was also reported for synthetic goethite containing ~4–5 mole % Al (Schwertmann *et al.*, 1985).

Activation-energy values for Ni-substituted hematite increased systematically with the incorporation of Ni (E = 16.7 + 0.67 (mole % Ni), r^2 = 0.77). This is not consistent with the smaller Ni-O bond energy relative to the Fe-O bond (Table 2) and may reflect the influence of other stereochemical properties of Ni^{2+} as well as the effect of the coupled substitution discussed above. Alternatively, the increase in E (Table 3) may reflect the improved structural ordering of Ni-substituted hematite as indicated by the increase in crystallite size along the [100] and [001] directions with increasing Ni content (Table 1).

Frequency-factor values for Mn-substituted hematites and for hematite containing 2.4 and 6.0 mole % Ni were comparable to values of A reported for synthetic hematite (A = 2.1×10^{10} $gFe/m^2/h$), of a similar size and shape, dissolved in 0.5 M HCl (Sidhu *et al.*, 1981). Values of A for Al- and Ni-bearing hematites varied by up to several orders of magnitude (Table 3). Similar variations in the magnitude of A were reported for synthetic goethites with Cr contents of ≤12 mole % (Lim-Nunez and Gilkes, 1987). In this case, the high A values were related to extensive etch-pit development during goethite dissolution.

Frequency-factor values for Al-, Mn-, and Ni-bearing hematite followed a trend similar to the changes in E (Table 3) with increasing metal content. The high frequency factor for hematite containing 8.3 mole % Al was not sufficient to offset the high activation energy for this sample, which had the lowest rate of dissolution (Table 3). The same result was shown for hematites containing 6.3 and 6.0 mole % Mn and Ni, respectively (Table 3).

Frequency-factor values for Al- and Ni-substituted hematite were unrelated to surface-area or other crys-

https://doi.org/10.1346/CCMN.2001.0490105 Published online by Cambridge University Press

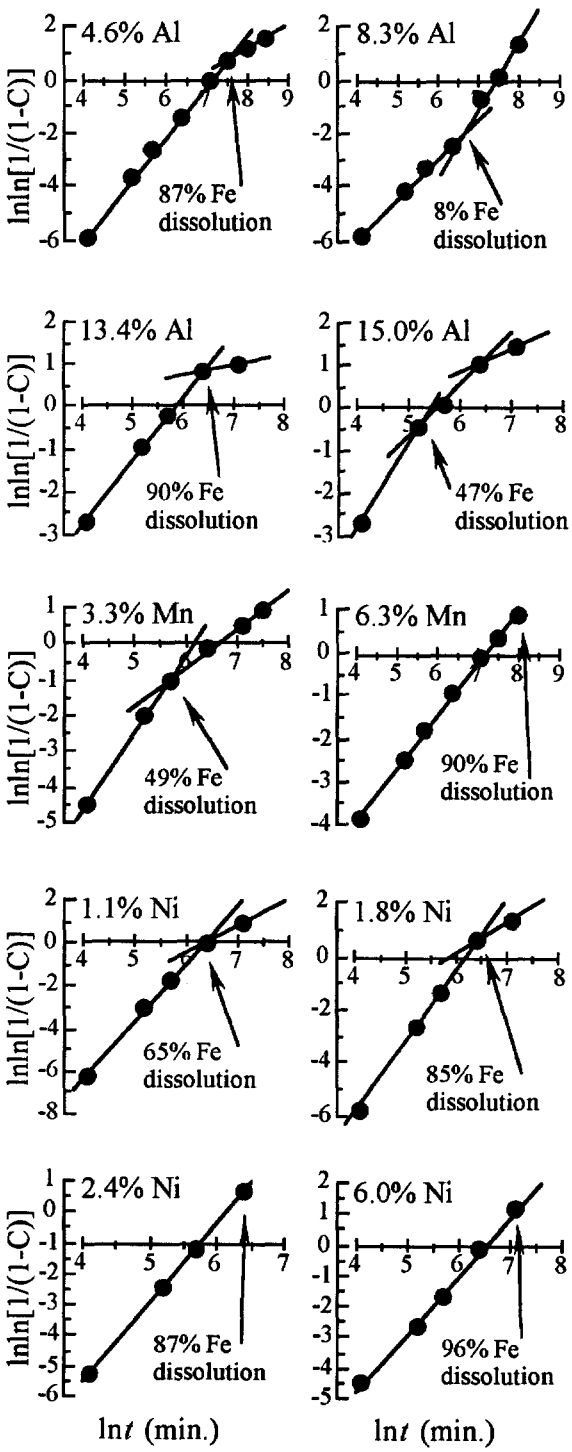

Figure 4. Linearized plots of the percentage of total Fe dissolved *versus* time for metal-substituted hematites fitted to the rate equation of Kabai (1973). An arrow indicates the percentage dissolution at which dissolution kinetics may cease to be fully described by the equation.

tal-shape parameters (*e.g.*, MCL_a, MCL_c). This result may reflect differences in the mode of acid attack of platy Al-bearing hematites as compared to equant Ni- (and Mn) substituted hematites. Hematite containing Al shows a morphology with predominantly basal (*e.g.*, 001) crystal surfaces, whereas Mn- and Ni-bearing hematite shows mainly non-basal (*e.g.*, 110) and basal surfaces (Figure 1).

Phosphate-adsorption studies (Barrón *et al.*, 1988; Colombo *et al.*, 1994) and microscopic examination of partially dissolved, unsubstituted synthetic and natural specular hematite have shown that basal (001) and near-basal (104) faces, having two- and three-fold coordinated surface-OH groups, were relatively unreactive compared to non-basal, prismatic faces (Hendewerk *et al.*, 1986; Maurice *et al.*, 1995). Mono-coordinated OH-surface groups present over non-basal (110) faces represent energetically more favorable sites for hematite dissolution (Barrón *et al.*, 1988; Cornell and Giovanoli, 1993). The difference in morphology (*i.e.*, aspect ratio) between platy and rhomboidal particles and presumably, difference in the number and nature of surface sites active in dissolution may account for variations in frequency factors between hematite containing Al and Mn- or Ni-substituted hematite. Frequency-factor values for Al-substituted hematite, with predominantly basal surfaces of less reactive dissolution sites, decreased with increasing Al content. In contrast, Mn- and Ni-substituted hematites, which show a rhomboidal crystal form with energetically more favorable sites for dissolution, showed an increase in values of A with increasing Mn and Ni contents.

TEM examination

Electron microscopic examination (Figure 5) of partially dissolved (~35 mole % Fe dissolved) Al-bearing hematite showed that dissolution mostly occurred at sites on basal surfaces with pit and hole formation developing normal to the basal surface (*i.e.*, parallel to the [001] direction) for hematite with a low Al content (Figure 5a and 5b). Similar hole formation was noted for platy soil hematite (Schwertmann, 1991) and synthetic hematite (Cornell and Giovanoli, 1993), and was thought to be initiated at screw-dislocation sites distributed over the basal surface (Sunagawa, 1962; Cornell and Giovanoli, 1993). Dissolution of hematite containing 15 mole % Al occurred mostly by edge attack (Figure 5c). The change in morphology of partially dissolved Al-bearing hematite owing to hole formation and micro-fracture development would increase the surface area exposed to proton attack thereby accelerating the rate of dissolution, which accounts for the dissolution curves (Figure 2).

Dissolution of rhomboidal Mn- and Ni-substituted hematite involved the rounding of corners and edges producing 'clover-leaf-like' forms (Figure 5). This ap-

https://doi.org/10.1346/CCMN.2001.0490105 Published online by Cambridge University Press

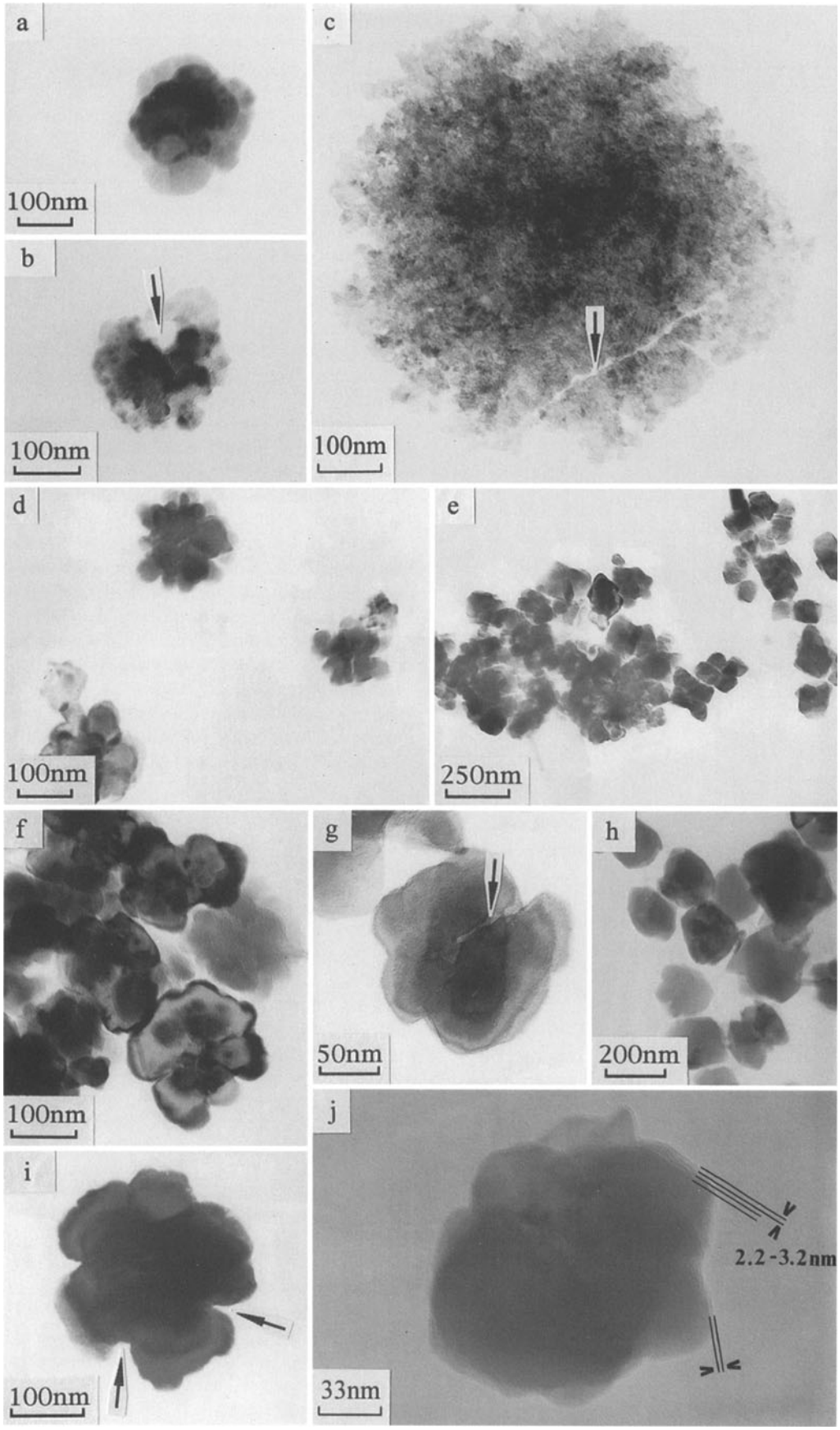

https://doi.org/10.1346/CCMN.2001.0490105 Published online by Cambridge University Press

pears to have resulted from preferred dissolution occurring at domain boundaries and by edge attack. Dissolution channels also developed, possibly occurring along micro-fractures, at areas of strain, or at domain boundaries (Figure 5g). Features such as twin boundaries, kinks, micro-fractures, and dislocations represent more active sites for dissolution (Berner, 1978; Meike, 1990). This change in morphology for Mn- and Ni-containing hematites during dissolution would also have increased the surface area susceptible to acid attack and explains the inhomogeneous dissolution (Figure 2). TEM micrographs of hematite after longer periods of dissolution are unavailable.

Recent microtopographical examination of specular hematite, using atomic force microscopy (AFM) and scanning tunnelling microscopy (STM), revealed the presence of etch pits and steps on basal surfaces with steps occurring every 2.0–3.0 nm (Heil *et al.,* 1989; Johnsson *et al.,* 1991; Eggleston and Hochella, 1992). Step edges develop parallel to the main crystal edge with step heights being typically one to two oxygen atomic layers high (Johnsson *et al.,* 1991).

High resolution TEM (HRTEM) of partially dissolved (~35 mole % Fe dissolved) Ni-substituted hematite showed the presence of similar features developed at crystal edges (Figure 5j). These step-terrace sequences have one step occurring every 2.2–3.2 nm. These sequences are consistent with reported observations (Heil *et al.,* 1989; Johnsson *et al.,* 1991; Eggleston and Hochella, 1992), and were not evenly developed over the crystal surface (Figure 5j). AFM examination of partially dissolved synthetic hematites also showed dissolution occurring at step edges and via etch-pit formation (Maurice *et al.,* 1995).

Lattice imaging of step-terrace sequences has indicated that O^{2-} ions at the hematite surface may relax to form a regular hexagonal array at step-edge terminations (Johnsson *et al.,* 1991; Eggleston and Hochella, 1992). Such a relaxation mechanism may explain preferential dissolution at corners and crystal edges. Relaxation of the bulk hematite structure at step-edge terminations, which are regions of incomplete coordination, may involve a localized reduction in activation energy and/or an increased density of dissolution sites so that preferential dissolution proceeds along a continually retreating step edge.

Metal distribution in hematite

Plots of the % metal (Me) dissolved *versus* % Fe dissolved during dissolution provides an indirect measure of the distribution of metal ions within the structure of Fe oxides (Sidhu *et al.,* 1981; Lim-Nunez and Gilkes, 1987; Cornell *et al.,* 1992). Convex or concave % Me:% Fe curves indicate accumulation of the incorporated metal at the surface or towards the center of Fe-oxide crystals, respectively. A straight line of unit slope intersecting the origin suggests that metal ions are uniformly incorporated within the Fe oxide (Sidhu *et al.,* 1981).

The concave % Al:% Fe curve for hematite containing 4.6 mole % Al indicates that Al tends to be concentrated towards the center relative to the surface of hematite particles (Figure 6). As the amount of Al substitution increased, Al is more uniformly distributed within hematite (Figure 6). Manganese and nickel were nearly uniformly distributed (Figure 6), so that the anisotropic dissolution of these hematites is not associated with local concentrations of these metals at crystal surfaces or at intergrain boundaries. Cornell *et al.* (1992) also demonstrated the near uniform incorporation of Ni in hematite prepared under conditions similar to those used here.

For hematite formed by the oxidation of Mn- and Ni-substituted magnetite, Mn also was nearly uniformly distributed within hematite, whereas Ni was concentrated near the surface of hematite (Sidhu *et al.,* 1980). This difference for Ni indicates an influence of synthesis procedure. During the oxidation of Ni-substituted magnetite via the reaction, Ni-rich magnetite $\xrightarrow{220°C}$ Ni-rich maghemite $\xrightarrow{650°C}$ Ni-rich hematite (Sidhu *et al.,* 1980), surface concentration of Ni for such hematites may result from the induced high-temperature diffusion of Ni^{2+} ions to the surface of the crystals. The increased crystallinity (*i.e.,* improved structural order) of 'heat-treated' or annealed hematite may cause the structure to be less accommodating of Ni than for hematite produced at room temperature from Ni-rich ferrihydrite.

The tendency of metal ions to be uniformly concentrated within hematite provides a measure of the ease of incorporation during hematite synthesis. Incorporation of metal ions within hematite, formed by a sol-

←

Figure 5. Transmission electron micrographs of partially dissolved (*i.e.,* ~35 mole % Fe dissolved) (a,b) low Al-, (c) high Al-; (d) low Mn-, (e) high Mn-; (f,g) low Ni-, and (h,i,j) high Ni-substituted hematites. Preferential dissolution of hematite containing 15.0 mole % Al involved the etching of micro-fractures (c-arrowed). Hole formation parallel to the [001] direction occurred for hematite with an Al content of 4.6 mole % (note arrow in b). Dissolution of more equant hematite containing 6.0 mole % Ni at domain boundaries resulted in formation of 'clover-leaf-like' forms (note arrows in i), or particles having lobed crystal edges as shown for hematite containing Mn (d,e). Development of micro-fissures at domain boundaries for hematites with 1.1 mole % Ni is also evident (note arrow in g). HRTEM of hematite with 6.0 mole % Ni (j) shows development of step-terrace sequences, which may act as sites of preferred dissolution.

https://doi.org/10.1346/CCMN.2001.0490105 Published online by Cambridge University Press

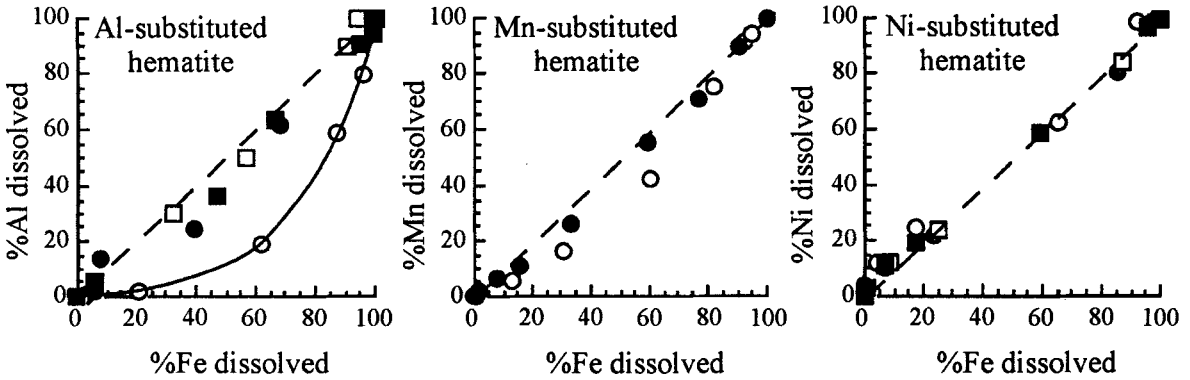

Figure 6. Plots of % of total metal dissolved *versus* % of total Fe dissolved for Al-, Mn-, and Ni-substituted hematites. Lines of unit slope – – – indicate uniform incorporation of metal ions within hematite. Legend symbols: Al-substituted hematites (○) 4.6 mole %, (●) 8.3 mole %, (□) 13.4 mole %, (■) 15.0 mole %; Mn-substituted hematites (○) 3.3 mole %, (●) 6.3 mole %; Ni-substituted hematites (○) 1.1 mole %, (●) 1.8 mole %, (□) 2.4 mole %, (■) 6.0 mole %.

id-solution reaction within ferrihydrite, is influenced *inter alia,* by the various ionic properties of the ions including size, electronegativity, and crystal-field stabilization energy (CFSE). At low metal contents of ~5–6 mole %, the sequence of metal incorporation within hematite is: (Fe) > Al > Mn ≈ Ni, with Al and, to a minor extent, Mn being relatively concentrated towards the center of crystals. As the amount of metal substitution increases, Al, Mn, and Ni are uniformly incorporated within hematite (Figure 6). This result is somewhat unexpected for Ni. Favorable CFSE and octahedral site-preference energies of Ni^{2+} may have opposed the effects of the smaller ionic charge and larger size of Ni^{2+} relative to Fe^{3+} (Table 3), which results in the near uniform distribution of Ni^{2+} within hematite.

CONCLUSIONS

Changes in unit-cell dimensions of hematite resulting from the incorporation of Al^{3+}, Mn^{3+}, and Ni^{2+} were consistent with the size of the ion that replaced Fe^{3+}. These ions were essentially uniformly incorporated within hematite so that the incongruent dissolution of Al-, Mn-, and Ni-substituted hematite did not result from localized concentrations of substituents acting as nuclei for dissolution at surface sites of subgrain boundaries.

The Cube Root Law and the rate equation of Kabai (1973) did not apply to the dissolution metal-substituted hematite in the present study. Instead, the Avrami-Erofe'ev rate equation successfully described the incongruent dissolution of most of the Al-, Mn-, and Ni-substituted hematites investigated. The dissolution rate, k, derived from the Avrami-Erofe'ev equation, of hematite containing Al was positively related to SA, whereas the rate of dissolution for Mn- and Ni-substituted hematites was unrelated to SA. This is in contrast to the findings of previous investigations where the dissolution rate of hematite was independent of morphology, with k directly proportional to SA (Cornell and Giovanoli, 1993). The plate-like morphology of Al-substituted hematite was essentially unchanged during the initial stage of dissolution (*i.e.,* ~35 mole % Fe dissolved). Instead, dissolution of original, rhomboidal Mn- and Ni-bearing hematites produced 'clover-leaf-like' forms. Hematite with essentially the same SA had distinctly different rates of dissolution.

Dissolution of metal-substituted hematites was not simply controlled by surface area *per se,* but was mediated by the combined influence of direct (*i.e.,* metal-oxygen bond energy, crystallinity) and indirect (*i.e.,* crystal size and shape) affects associated with incorporation of metal ions within hematite. Differences in the rate and mode of acid attack relate to the nature (*i.e.,* coordination) of reactive sites on different crystal surfaces of Al- and Ni-substituted hematites. Development of non-basal (*e.g.,* 110) faces, with sites more energetically favorable for dissolution were reflected in the very high frequency-factor values for hematite containing Ni (and Mn). The low frequency-factor values for Al-substituted hematite reflected their plate-like morphology, consisting of predominantly basal (*i.e.,* 001) surfaces with sites relatively unreactive to acid attack. However, the high SA and poorer crystallinity of Al-bearing hematites resulted in a low activation energy despite the larger Al-O bond energy, with the overall effect of increasing the rate of dissolution.

ACKNOWLEDGMENTS

The authors gratefully acknowledge the assistance of P. Butterworth, at the CSIRO Division of Soils Adelaide, S.A., in performing the surface-area determinations. Thanks are also extended to two anonymous reviewers and to S. Guggenheim for their helpful suggestions and comments.

REFERENCES

Azuma, K. and Kametani, H. (1964) Kinetics of dissolution of ferric oxide. *Transactions of the Metallurgical Society of AIME,* **230,** 853–862.

Barrón, V., Herruzo, M., and Torrent, J. (1988) Phosphate adsorption by aluminous hematites of different shapes. *Journal of the Soil Science Society of America,* **52,** 647–651.

Baumgartner, E., Blesa, M.A., Marinovich, H., and Maroto, A.J.G. (1983) Heterogeneous electron transfer as a pathway in the dissolution of magnetite in oxalic acid solutions. *Inorganic Chemistry,* **22,** 2226–2228.

Berner, R.A. (1978) Rate control of mineral dissolution under earth surface conditions. *American Journal of Science,* **278,** 1235–1252.

Burns, R.G. (1970) *Mineralogical Applications of Crystal Field Theory.* Cambridge University Press, 224 pp.

Colombo, C., Barrón, V., and Torrent, J. (1994) Phosphate adsorption and desorption in relation to morphology and crystal properties of synthetic hematites. *Geochimica et Cosmochimica Acta,* **58,** 1261–1269.

Cornell, R.M. and Giovanoli, R. (1989) Effect of cobalt on the formation of crystalline iron oxides from ferrihydrite into goethite and hematite in alkaline media. *Clays and Clay Minerals,* **37,** 65–70.

Cornell, R.M. and Giovanoli, R. (1993) Acid dissolution of hematites of different morphologies. *Clay Minerals,* **28,** 223–232.

Cornell, R.M. and Schindler, P.W. (1987) Photochemical dissolution of goethite in acid/oxalate solution. *Clays and Clay Minerals,* **35,** 347–352.

Cornell, R.M., Posner, A.M., and Quirk, J.P. (1974) Crystal morphology and the dissolution of goethite. *Journal of Inorganic and Nuclear Chemistry,* **36,** 1937–1946.

Cornell, R.M., Posner, A.M., and Quirk, J.P. (1975) The complete dissolution of goethite. *Journal of Applied Chemical Biotechnology,* **25,** 701–706.

Cornell, R.M., Posner, A.M., and Quirk, J.P. (1976) Kinetics and mechanisms of the acid dissolution of goethite (α-FeOOH). *Journal of Inorganic and Nuclear Chemistry,* **38,** 563–567.

Cornell, R.M., Giovanoli, R., and Schindler, P.W. (1987) Effect of silicate species on the transformation of ferrihydrite into goethite and hematite in alkaline media. *Clays and Clay Minerals,* **35,** 21–28.

Cornell, R.M., Giovanoli, R., and Schneider, W. (1992) The effect of nickel on the conversion of amorphous iron (III) hydroxide into more crystalline iron oxides in alkaline media. *Journal of Chemistry and Technical Biotechnology,* **53,** 73–79.

Davies, S.R.H. and Morgan, J.J. (1989) Manganese (II) oxidation kinetics on metal oxide surfaces. *Journal of Colloid and Interface Science,* **129,** 63–77.

DeGrave, E., Bowen, L.H., Amarasiriwarden, D.D., and Vandenberghe, R.E. (1988) ^{57}Fe Mössbauer effect study of highly substituted aluminum hematites: Determination of the magnetic hyperfine field distributions. *Journal of Magnetism and Magnetic Materials,* **72,** 129–140.

Eggleston, C.M. and Hochella, M.F., Jr. (1992) The structure of the hematite {001} surface by scanning tunneling microscopy: Image interpretation, surface relaxation, and step structure. *American Mineralogist,* **77,** 911–922.

Fischer, W.R. and Schwertmann, U. (1975) The formation of hematite form amorphous iron (III) hydroxide. *Clays and Clay Minerals,* **23,** 33–37.

Giovanoli, R. and Cornell, R.M. (1992) Crystallization of metal-substituted ferridydrites. *Zeitschrift Pflanzenernährung Bodenkunde,* **129,** 63–77.

Handbook of Chemistry and Physics (1988) Table 1. Bond strengths in diatomic molecules. R. Weast, ed., CRC Press Inc., Florida, F-115.

Heil, J., Wesner, J., Lommel, B., Assmus, W., and Grill, W. (1989) Structural investigations of surfaces of blue bronze and hematite by scanning tunneling microscopy. *Journal of Applied Physics,* **65,** 5220–5222.

Hendewerk, M., Salmeron, M., and Somorjai, G.A. (1986) Water adsorption on the (001) plane of Fe_2O_3: An XPS, UPS, Auger, and TPD study. *Surface Science,* **172,** 544–556.

Jeanroy, E., Rajot, J.L., Pillon, P., and Herbillon, A. (1991) Differential dissolution of hematite and goethite in dithionite and its implication on soil yellowing. *Geoderma,* **50,** 79–94.

Johnnson, P.A., Eggleston, C.M., and Hochella, M.F., Jr. (1991) Imaging molecular-scale structure and microtopography of hematite with the atomic force microscope. *American Mineralogist,* **76,** 1442–1445.

Johnston, J.H. and Lewis, D.G. (1983) A detailed study of the transformation of ferrihydrite to hematite in an aqueous medium at 92°C. *Geochimica et Cosmochimica Acta,* **41,** 1823–1831.

Kabai, J. (1973) Determination of specific activation energies of metal oxides and metal oxide hydrates by measurement of the rate dissolution. *Acta Chimica Academiae Scientarum Hungaricae,* **78,** 57–73.

Klug, H.P. and Alexander, L.E. (1974) *X-ray Diffraction Procedures for Polycrystalline and Amorphous Materials.* John Wiley and Sons, New York, 996 pp.

Krestov, G.A., Shormanov, V.A., and Pimenova, N.I. (1973) Kinetic study of the dissolution of α-iron (III) oxide in aqueous solutions of inorganic acids. *Izvestiya Vysshikh Uchebnykh Zavedenii, Khimiya i Khimicheskaya Tekhnologiya,* **16,** 377–381.

Kuhnel, R.A. (1987) The role of cationic and anionic scavengers in laterite. *Chemical Geology,* **60,** 31–40.

Lim-Nunez, R. and Gilkes, R.J. (1987) Acid dissolution of synthetic metal-containing goethites and hematites. In *Proceedings of the International Clay Conference, 1985, Denver,* L.G. Schulze, H. van Olphen, and F.A. Mumpton, eds., Clay Minerals Society, Bloomington, Indiana, 197–204.

Macedo, J. and Bryant, R.B. (1989) Preferential microbial reduction of hematite over goethite in a Brazilian oxisol. *Journal of the Soil Science Society of America,* **53,** 1114–1118.

Maurice, R.A., Hochella, M.F., Jr., Parks, G.A., Sposito, G., and Schwertmann, U. (1995) Evolution of hematite surface microtopography upon dissolution by simple organic acids. *Clays and Clay Minerals,* **43,** 29–38.

McKeague, J.A. and Day, J.H. (1966) Dithionite- and oxalate-extractable Fe and Al as aids in differentiating various classes of soils. *Canadian Journal of Soil Science,* **46,** 13–22.

Meike, A. (1990) A micromechanical perspective on the role of dislocations in selective dissolution. *Geochimica et Cosmochimica Acta,* **54,** 3347–3352.

Melville, M.D. and Atkinson, G. (1985) Soil colour: Its measurement and its designation in models of uniform colour space. *Journal of Soil Science,* **36,** 495–512.

Novak, G.A. and Colville, A.A. (1989) A practical interactive least squares cell-parameter program using an electronic spreadsheet and a personal computer. *American Mineralogist,* **74,** 488–490.

Pryor, M.J. and Evans, U.R. (1950) The reductive dissolution of ferric oxide in acid. Part I. The reductive dissolution of oxide films present on iron. *Journal of the Chemical Society,* 1259–1266.

Schwertmann, U. (1984) The influence of aluminium on iron oxides. IX. Dissolution of Al-goethite in 6M HCl. *Clay Minerals,* **19,** 9–19.

Schwertmann, U. (1991) Solubility and dissolution of iron oxides. *Plant and Soil,* **130,** 1–25.

Schwertmann, U. and Murad, E. (1983) Effect of pH on the formation of goethite and hematite from ferrihydrite. *Clays and Clay Minerals,* **31,** 277–284.

Schwertmann, U. and Taylor, R.M. (1989) Iron oxides. In *Minerals in Soil Environments,* J.B. Dixon and S.B. Weed, eds., Soil Science Society of America, Madison, Wisconsin, USA, 379–438.

Schwertmann, U., Fitzpatrick, R.W., Taylor, R.M., and Lewis, D.G. (1979) The influence of aluminum on iron oxides. Part II. Preparation and properties of Al-substituted hematites. *Clays and Clay Minerals,* **27,** 105–112.

Schwertmann, U., Cambier, P., and Murad, E. (1985) Properties of goethite of varying crystallinity. *Clays and Clay Minerals,* **33,** 369–378.

Segal, M. and Sellers, R. (1980) Reduction of solid iron (III) oxides with aqueous reducing agents. *Journal of the Chemical Society and Chemical Communications,* 991–993.

Shannon, R.D. (1976) Revised effective ionic radii and systematic studies of inter-atomic distances in halides and chalcogenides. *Acta Crystallographica,* **A32,** 751–767.

Sidhu, P.S., Gilkes, R.J., and Posner, A.M. (1980) The behaviour of Co, Ni, Zn, Cu, Mn and Cr in magnetite during alteration to maghemite and hematite. *Journal of the Soil Science Society of America,* **44,** 135–138.

Sidhu, P.S., Gilkes, R.J., Cornell, R.M., Posner, A.M., and Quirk, J.P. (1981) Dissolution of iron oxides and oxyhydroxides in hydrochloric and perchloric acids. *Clays and Clay Minerals,* **29,** 269–276.

Stanjek, H. and Schwertmann, U. (1992) The influence of aluminium on iron oxides. Part XVI: Hydroxyl and aluminium substitution in synthetic hematites. *Clays and Clay Minerals,* **40,** 347–354.

Sulzberger, B., Suter, D., Siffert, C., Banwart, S., and Stumm, W. (1989) Dissolution of Fe(II) (hydr) oxides in natural waters; Laboratory assessment on the kinetics controlled by surface coordination. *Marine Chemistry,* **28,** 127–144.

Sunagawa, I. (1962) Mechanism of natural etching of hematite crystals. *American Mineralogist,* **47,** 1332–1345.

Surana, V.S. and Warren, I.H. (1969) The leaching of goethite. *Transactions of the Institute of Mining and Metallurgy,* **80,** C152–155.

Torrent, J., Schwertmann, U., and Barrón, V. (1987) The reductive dissolution of synthetic goethite and hematite by dithionite. *Clay Minerals,* **22,** 329–337.

Vandenberghe, R.E., Verbeeck, A.E., DeGrave, E., and Stiers, W. (1986) ^{57}Fe Mössbauer effect study of Mn-substituted goethite and hematite. *Hyperfine Interactions,* **29,** 1157–1160.

Warren, I.H. and Roach, G.I.D. (1971). Physical aspects of the leaching of goethite and hematite. *Transactions of the Institute of Mining and Metallurgy,* **80,** C151–155.

Warren, I.H., Bath, M.D., Posner, A.P., and Armstrong, J.T. (1969) Anisotropic dissolution of hematite. *Transactions of the Institute of Mining and Metallurgy,* **78,** C21–27.

Wells, M.A., Gilkes, R.J., and Anand, R.R. (1989) The formation of corundum and aluminous hematite by the thermal dehydroxylation of aluminous goethite. *Clay Minerals,* **24,** 513–530.

E-mail of corresponding author: m.wells@per.dem.csiro.au

(Received 26 August 1999; accepted 12 August 2000; Ms. 374; A.E. Helge Stanjek)